A Study of the Interaction of Carbon Rich Polymer Nanodots with Serum Albumins: A Spectroscopic Investigation

M.Sc. Thesis

By
Somnath Das

DISCIPLINE OF CHEMISTRY

INDIAN INSTITUTE OF TECHNOLOGY INDORE

June 2016

A Study of the Interaction of Carbon Rich Polymer Nanodots with Serum Albumins: A Spectroscopic Investigation

A Thesis

Submitted in partial fulfilment of the

requirements for the award of the degree

of

MASTER OF SCIENCE

by

Somnath Das

DISCIPLINE OF CHEMISTRY

INDIAN INSTITUTE OF TECHNOLOGY INDORE

June 2016

INDIAN INSTITUTE OF TECHNOLOGY INDORE

CANDIDATE'S DECLARATION

I hereby certify that the work which is being presented in the thesis entitled as **"A Study of the Interaction of Carbon Rich Polymer Nanodots with Serum Albumins: A Spectroscopic Investigation"** in the partial fulfilment of the requirements for the award of the degree of **MASTER IN SCIENCE** and submitted in the **DISCIPLINE OF CHEMISTRY, INDIAN INSTITUTE OF TECHNOLOGY INDORE**, is an authentic record of my own work carried out during the time period from July 2015 to June 2016 of my M.Sc programme and submitted under the supervision of **Dr. Tushar Kanti Mukherjee**, Associate Professor, Indian Institute of Technology Indore.

The matter presented in this thesis has not been submitted by me for the award of any other degree of this or any other institute.

Somnath Das

This is to certify that the above statement made by the candidate is correct to the best of my knowledge.

Dr. Tushar Kanti Mukherjee

Mr. Somnath Das has successfully given his **M.Sc Oral Examination** held on 7th July, 2016.

Signature of Thesis Supervisor Date:	Signature of Convener DPGC Date:
Signature of PSPC Member #1 Date:	Signature of PSPC Member #2 Date:

ACKNOWLEDGEMENTS

First and foremost, I would like to express my profound gratitude and deep regards to my mentor cum thesis supervisor Dr. Tushar Kanti Mukherjee for his exemplary guidance, monitoring and constant encouragement through this journey and making my research experience productive and stimulating. It has been an honour for me to be one of his first M.Sc project students. His joy and enthusiasm for research always keep me motivated during many tough moments of this project. I also take this opportunity to express a deep sense of gratitude towards our Director, Prof. Pradeep Mathur and head of Chemistry discipline Dr. Satya S. Bulusu for constantly motivating us for research and providing various facilities, which helped me to focus on the project exclusively.

I am very grateful towards my PSPC committee members Dr. Anjan Chakraborty and Dr. Satyajit Chatterjee and DPGC convener Dr. Apurba K. Das for their valuable suggestions and encouragement. I am very much obliged to Sophisticated Instrument Center (SIC) of IIT Indore for instrumental facilities, all the faculty members and stuffs of discipline of chemistry and also technicians, librarians of IIT Indore for their constant help and support. Especially, Mr. Manish Kushwaha and Mr. Kinny Punday for helping during CD spectrometer study.

I express my sincere regards to Mr. Arpan Bhattacharya for being supportive and guiding me as a brother at each and every stage of this project. I am also grateful to my lab mates Dr. Vijaykant Khorwal, Mr. Surajit Chatterjee, Ms. Roopali Prajapati, Ms. Jamuna Vaishnav and Ms. Bhaswati Sarkar for their moral support and active co-operation during my lab work. I also convey my heartfelt gratitude towards all of my friends, juniors, seniors and Ph.D. scholars specially Mr. Ajay, Mr. Sarthak Mishra, Mr. Jonu Yadav, Mr. Rahul Sharma, Ms. Ritu Chahal, Ms. Jyotshna Tyagi, Ms. Namrata Khadsang. Ms. Gurpreet Kaur, Mr.

Deepu Kumar, Mr. Piyush Kumar Goutam, Mr. Haardik Panday, Mr. Anupam Das, Mr. Sagnik Sengupta, Ms. Manideepa Saha, Mr. Rajendra Nasni, Mr. Chandan Adhikari, Ms. Sonam Mandani, Ms. Neha Thakur, Mr. Siddarth Jain, Mr. Sagar Biswas, Mr. Bishnu Basu Giri, Mr. Ankan Biswas, Mr. Sahidul Mandal, Mr. Mriganka Das, Ms. Poulami Mondal, Mr. Biju Majumdar Dr. Bhagwata Sharma, Mr. Debasish Majee, Mr. Bidyut Rana Kundu and Mr. Sayan Maiti for their co-operation.

Finally, I also thanks to my parents, family members and relatives for their unconditional support, encouragement, love, prayers and patience without which it would not have been possible to achieve.

There are many more people who have contributed in their own ways, hope I could thank all of them, but time and space compel me to stop here.

7th July, 2016 **Somnath Das,**

IIT Indore

Dedicated to my

Grandfather

For being my first Teacher

ABSTRACT

Here, we investigate the interaction of carbon rich polymer nanodots (PNDs) with bovine serum albumin (BSA) and human serum albumin (HSA) under physiological conditions by means of fluorescence spectroscopy, circular dichroism (CD) and FT-IR spectroscopy. It has been observed that the steady-state fluorescence quenching of BSA and HSA by PNDs is a result of ground state complex formation and this leads to static quenching mechanism which is further supported by lifetime measurements. The binding parameters are estimated from Stern-Volmer and Scatchard equation. The binding constant of both the albumins with PNDs is in the order of 10^5 M^{-1}. The calculated thermodynamic parameters reveal that the enthalpy change (ΔH) and entropy change (ΔS) are negative and these results have been explained by considering specific hydrogen bonding (H- bonding) interactions between amine ($–NH_2$) and hydroxyl (-OH) groups of PNDs and carboxylate ($–COO^-$) groups of aspartate (Asp) and glutamate (Glu) residues of BSA/HSA. Moreover, salt effect study confirms that, electrostatic interaction doesn't play any role in the protein-PNDs association process. The observed H-bonding interaction is spontaneous since the overall free energy change (ΔG) is negative. Competitive experiments using warfarin and ibuprofen as site markers indicate that association of BSA and HSA with PNDs occurs selectively through site I of the proteins. Furthermore, the CD spectral analysis indicates that the secondary structure of BSA/HSA changes considerably in the presence of PNDs probably due to partial unfolding of the albumins proteins at the nanoparticle surface, although the overall tertiary structure remains intact.

TABLE OF CONTENTS

LIST OF FIGURES

LIST OF SCHEMES

LIST OF TABLES

NOMENCLATURES

ΔH	Enthalpy Change
ΔG	Free energy change
ΔS	Entropy change
Å	Angstrom
kDa	Kilodalton
mL	Milliliter
µM	Micromolar
mm	millimetre
nm	Nanometer
ns	Nanosecond
R	Universal Gas Constant
ps	Picosecond
mV	Millivolt
pH	$-\log_{10}[H^+]$
mM	Millimolar
M	Molecular Weight
ϕ	Quantum Yield
I	PL Intensity

η	Refractive Index
l	Path Length
A	Absorbance (optical density, OD)
ε	Molar Extinction Coefficient
τ	Average Lifetime
a_i	Lifetime Components
χ^2	Fitting Parameter
λ	Wavelength
K_{sv}	Stern-Volmer Constant
K_q	Bimolecular Quenching Constant
Q	Quencher
K_b	Binding Constant
n	Number of Binding sites
R^2	Correlation Coefficient
kV	Kilovolt

ACRONYMS

CNDs	Carbon Nanodots
PNDs	Polymer Nanodots
HSA	Human Seram Albumin
CDs	Carbondots
BSA	Bovine Serum Albumin
CD	Circular Dichroism
FT-IR	Fourier Transfer Infrared
MWCO	Molecular Weight Cut-off
Asp	Aspartic Acid
Waf	Warfarin
QD	Quantum Dot
Ibu	Ibuprofen
PL	Photolumniscence
EDTA	Ethylenediamine Tetraacetic Acid
TEM	Transmission Electron Microscopy
NPs	Nanoparticles
Trp	Tryptophan
QY	Quantum Yield
SV	Stern-Volmer Plot
QS	Quinine Sulphate
UV-Vis	Ultraviolet Visible Spectroscopy
OD	Optical Density
PXRD	Powder X-Ray Diffraction
mdeg	Millidegree

MRE	Mean Residual Ellipticity
IRF	Instrument Response Function
TCSPC	Time Correlated Single Photon Counting

Chapter 1:

1.1 INTRODUCTION:

Fluorescent carbon nanodots (CNDs) are widely used in metal ion probes,*[1]* imaging,*[2]* optical sensors,*[3]* catalysis*[4]* and in the fields of energy*[5]* since their discovery in the year of 2004.*[6]* The photoluminescence (PL) of CNDs comes from quantum confinement effect along with different emissive trap states (defect states) on their surface. Unlike the traditional fluorescent semiconductor quantum dots *[7]*, CNDs overcome disadvantages such as toxicity, high-cost, larger size and undesirable oxidation that limits their biological applications. They also have excellent photostability, water solubility, easy functionalization as well as unique optical properties, which enables more practical applications. *[4,8,9]* In addition CNDs show excitation wavelength (λ_{ex}) and temperature dependent PL spectrum.*[10, 11]* Their potential application as an effective optical probes for the detection of Fe^{3+} and Cu^{2+} ions have been explored in the literature.*[12]* CNDs generally shows high quantum yield but most recently there are some reports where CNDs have low quantum yields (<10%) and low water-solubility, which are the challenges in synthesis.*[2, 13]* Nitrogen containing polymer nanodot (PNDs), due to their unique properties has been exclusively applied in various fields such as sensors*[14]*. superconductors*[15]* and lithium ion batteries.*[16]* Recently, much attention has been focused on the fluorescent N-doped polymer carbon nanodots (N-PNDs). They are a new kind of nanoscale particles with conjugated sp^2 hybridized and unsaturated sp^3 hybridized carbon atoms. *[17-18]* There are various methods reported in the literature such as reflux, microwaves and solvothermal heating for preparation of N-doped polymer nanodots.*[19]* PNDs can be obtained by heating organic compounds such as ethylenediaminetetraaceticacid (EDTA)*[20]*, glucosamine HCl*[21]*, amino acids*[22]* etc. Polymer

nanodots (PNDs) have also been produced from grass in a recent report. *[23-29]*. In the present work, we have spectroscopially investigated the effect of polymer nanodots with serum albumins in presence of two differently specific site markers.

Serum albumins are the most abundant proteins in blood plasma and also most widely studied proteins. They are extensively used in biophysical and biochemical studies as a model system for protein folding, aggregation and drug delivery.*[30]* The main role of serum albumins in psychological systems is disposition and transportation of various exogenous and endogenous compounds like drugs, fatty acids, hormones etc to the sites where its use.*[30]* Albumins are the biomacromolecules that are involved in the maintenance of colloid-blood pressure and are implicated in facilitating transfer of many ligands across the organ-circulatory interfaces such as liver, intestine, kidney and brain.*[31]* Two well known serum proteins are human serum albumin (HSA) and bovine serum albumin (BSA) and the structural aspects of them are well known. The primary structure of these proteins have about 580 amino acid residues which assume the solid equilateral triangular shape with sides ~ 80Å and depth ~30 Å and is characterised by a low content of tryptophan and a high content of cystine stabilizing a series of nine loops. The secondary structures of these serum albumins are constituted of ~67% of helix of 6 turns and 17 disulfide bridges.*[32,33]* Human and bovine serum albumins display approximately 80% sequential homology. The primary structure of BSA is composed of 583 amino acid residues consisting of two Tryptophan (Trp) residues (Trp-134 and Trp-212). From the spectroscopic point of view, one of the main differences between the two proteins is that HSA has only one tryptophan residue (Trp-214), whereas BSA has two tryptophan residues (Trp-134 and Trp- 212) at different locations. *[32, 33]* From the determined crystallographic structure of HSA, it is proposed that the single Trp residue (Trp-214) is located in IIA binding site (domain II). Helms *et al.* And El-Kemary *et al.* have

suggested that in the case of BSA, Trp-212 is located in a similar hydrophobic environment as the single Trp-214 in HSA (sub-domain IIA), whereas, Trp-134 is more exposed to solvent and it is localized in the sub-domain IB.*[34,35]* The tertiary structure of HSA/BSA is composed of three domains I, II and III. Each domain is constituted by two sub domains denoted as A and B. Since domains II and III share a common interface, binding of a probe to domain III leads to conformational changes affecting the binding affinities to domain II and vice-versa. The principal ligand binding sites are located in sub domain IIA, IIIA and it appears that in the HSA/BSA these sites are homologous, although, they differ in affinities. The specific delivery of ligands by serum albumins originates from the presence of two major and structurally selective binding sites, namely Sudlow's site I and site II, which are located in three homogeneous domains that form a heart-shaped structure. However, this assembling of the domains can be modified, depending on the environmental conditions. They also suggested that the serum proteins can adopt many conformations, ranging from a compact structure to a relaxed form.*[34,35]* It has been reported that ligands having higher affinity for site I binds through hydrophobic interaction whereas ligands possessing preferential binding affinity for site II binds through a combination of hydrophobic, electrostatic and hydrogen bonding interaction.*[36,37]* The structures of BSA and HSA are given in Fig. 1, showing different domains, sub-domains and the locations of the tryptophan units.

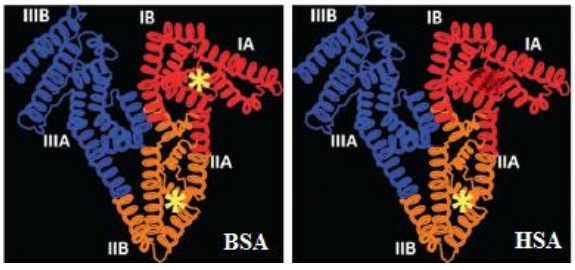

Fig. 1: Schematic representation of native BSA and HSA structure with relative positions of Trp moiety.

According to Sudlow's nomenclature, *[38, 39]* two primary sites (I and II) have been identified for ligand binding to BSA/HSA. Warfarin (Waf), an anticoagulant drug, and ibuprofen (Ibu), a nonsteroidal anti-inflammatory agent (see Table 1), have been considered as stereotypical ligands for Sudlow's site I and II, respectively. Warfarin, as other bulky heterocyclic anions, binds to site I, located in sub-domain IIA, whereas ibuprofen, as other aromatic carboxylates with an extended conformation, prefers site II, located in sub-domain IIIA.*[40]* Although the binding sites of BSA/HSA are well known but the interaction of PNDs with BSA/HSA has not been fully investigated.

Drug	Specificity towards BSA/HSA	Chemical formula	Molecular weight (gm/mole)	Structure
Warfarin	Site I	$C_{19}H_{16}O_4$	308	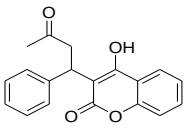 **warfarin**
Ibuprofen	Site II	$C_{13}H_{18}O_2$	206	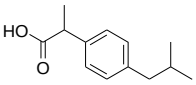 **ibuprofen**

Table 1: Structural formula and molecular weight of Warfarin and Ibuprofen.

In this project we present a spectroscopic analysis of the interaction of BSA and HSA with polymer nanodots at physiological conditions in the absence and presence of warfarin and ibuprofen as site markers.

Chapter 2:

EXPERIMENTAL SECTION:

2.1 Materials:

Glucose, glycine and Ibuprofen were purchased from TCI chemicals. Bovine serum albumin and Human serum albumin (BSA, HSA ≥99% essentially fatty acid free and globulin free), Tris, Warfarin, and Pur-A-Lyzer ™ Dialysis Kit (MWCO 3.5 kDa) were purchased from Sigma-Aldrich. All of the chemicals were used as received without further purification. Milli-Q water was obtained from a Millipore water purifier system (Milli-Q integral) and used thought out the experiments.

2.2 Synthesis of the polymer nanodots:

In a typical experiment, PNDs were synthesized according to the previously reported method *[41]* with slight modification (Scheme 1). Glucose (4.5g) and glycine (2.25g) were added to 30mL Milli-Q water. Then, the mixture was sealed into a Teflon-lined autoclave and heated at

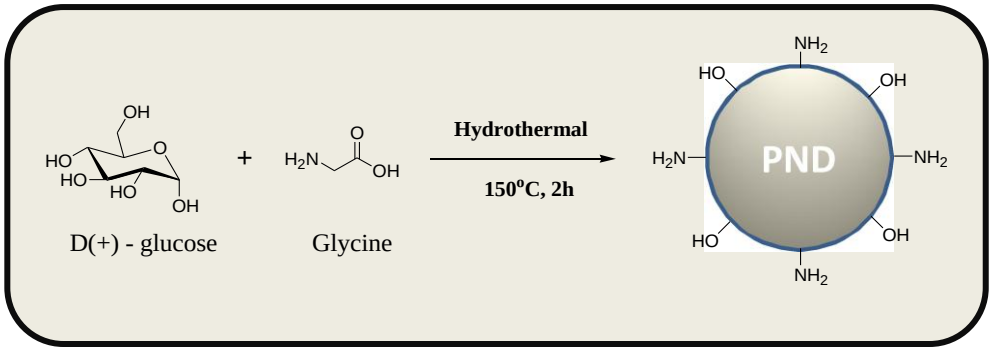

Scheme 1: Schematic representation of the synthesis of polymer nanodots using glucose (a reducing sugar) and glycine (an amino acid).

150^{o}C for 2h in a furnace. When cooled down to ambient temperature, a dark brown solution was obtained, which implied the formation of the PNDs. Then, they were filtered through a 0.2 µm Whatman filter membrane to remove the larger particles, and then dialyzed against Milli-Q water through a Pur-A-Lyzer ^{TM} Dialysis Kit with a molecular weight cut off of 3.5 kDa for 24 h. Finally, a brown aqueous solution containing PNDs was obtained. All the experiments were done with this PNDs.

2.3 Sample Preparation:

All the solutions were prepared in pH 7.4 Tris-HCl buffer (10 mM). BSA/HSA solutions of 1mM were prepared by dissolving 13 mg BSA/HSA (M_{BSA} = 66 kDa and M_{HSA} = 66.5 kDa) in 200 µL buffer and it was stored at low temperature in refrigerator. Separately warfarin (1mM) and ibuprofen (1mM) stock solutions were prepared by dissolving their crystals in tris-HCl buffer and diluting to the desired concentration.

2.4 Quantum Yield, Molar extinction coefficient and Concentration determination:

To determine the quantum yield (QY) of the synthesized PNDs it is require to match the absorbance of PNDs with a reference sample solution whose QY is already known. For this purpose a solution of Quinine Sulphate (QS) in the corresponding buffer was prepared and the QY of synthesized PNDs was estimated using quinine sulphate as reference according to the following equation. *[42]*

$$\phi_{PND} = \phi st\ (I_{PND}/I_{st})\ (\eta_{PND}/\eta_{st})^2\ (A_{st}/A_{PND})$$

where ϕ is the QY , I is the integrated PL intensity, η is the refractive index of the solvent, and A is the optical density (the absorbance value is below 0.10 at the excitation wavelength). The subscript ‘‘st’’ stands for standard and ‘‘PND’’ stands for the carbon rich N-doped polymer nanodot

sample. It was found that the QY of the sample is 8.4%. The molar extinction co-efficient (ϵ) of the PNDs was calculated from the ratio of its QY to the average life time i.e. ϕ_{PND} / τ_{PND}, where ϕ_{PND} is the QY and τ_{PND} is the average lifetime of the PNDs.*[43]* The molar extinction co-efficient (ϵ) is found to have around 3.28×10^3 M^{-1} cm^{-1}. After getting the ϵ value we have successfully determine the concentration of PNDs by using the well-known Lambert Beer's law.

2.5 Instrumentation:

Absorption spectra were recorded in a quartz cuvette (10×10 mm) using a Varian UV-Vis spectrophotometer (Carry 100 Bio). The fluorescence spectra were recorded in a quartz cuvette (10×10 mm) using a Fluoromax-4 Spectrofluorimeter (HORIBA Jobin Yvon, model FM-100) with an excitation and emission slit width of 2 nm. Since PNDs absorb light in the region 200-450 nm, all the PL spectra of PNDs are OD (optical density) corrected. *[44]* The PL spectra of PNDs was deconvoluted using Origin software. Circular Dichroism (CD) spectra were measured on a JASCO J-815 CD spectropolarimeter using a quartz cell of 1 mm path length. Scans were made with a slit width of 1 mm and speed of 20 nm min^{-1}. FTIR spectra were recorded for KBr pellets using a Bruker spectrometer (Tensor-27). Transmission electronmicroscopy (TEM) images were recorded on a JEOL electron microscope (JEM-2100 F) operating at an accelerating voltage of 200 kV. Samples were placed on a holey carbon lacey grid and air dried prior to imaging. For image analysis ImageJ (version 1.47v) by the National Institutes of Health (NIH) was used. PL decays were recorded on a HORIBA Jobin Yvon picosecond time correlated single photon counting (TCSPC) spectrometer (model Fluorocube-01-NL). The samples were excited at 278 nm using a picosecond diode laser (model Pico Brite-375L). The decays were collected using an emission polarizer at a magic angle of 54.7^o by a

photomultiplier tube (TBX-07C). The instrument response function (IRF, fwhm ~140 ps) was recorded using a dilute ludox solution. The fluorescence decays were analyzed using IBH DAS 6.0 software by the iterative reconvolution method, and the goodness of the fit was judged by a reduced χ-square (χ2) value. The decays were fitted with three exponential function:

$$F(t) = \sum_{i=1}^{3} a_i \exp(-t/\tau_i)$$

where $F(t)$ denotes normalized PL decay and a_1, a_2 and a_3 were the normalized amplitude of decay components t_1, t_2 and t_3, respectively. The average lifetime was obtained from the equation:

$$<\tau> = \sum_{i=1}^{3} a_i \tau_i$$

Chapter 3:

RESULTS AND DISCUSSION:

3.1 Characterisation of the PNDs:

The synthesized PNDs shows PL quantum yield of ~8.4% in tris-HCl buffer and it has a composition of 50.36% C, 5.22% H, 7.76% N and 36.66% O which was obtained from elemental analysis. The surface functional groups and the particle size of the PNDs are revealed by the FTIR spectroscopy and HR-TEM experiments. Fig. 2A shows the FTIR spectrum of the PNDs. The broad peak at around 3200-3550 cm^{-1} is assigned to the O-H and N-H moieties. The peak at 2922 cm^{-1} arises due to the C-H stretching vibrations. A prominent peak at 1632 cm^{-1} is basically due to the bending motions of the N-H moieties. The other

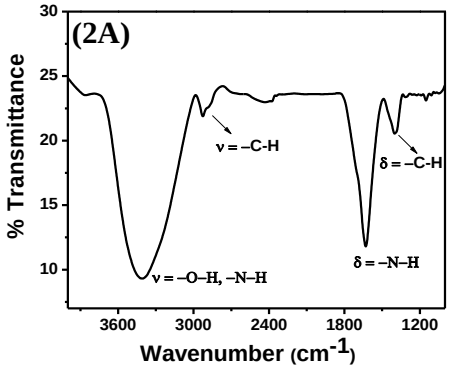

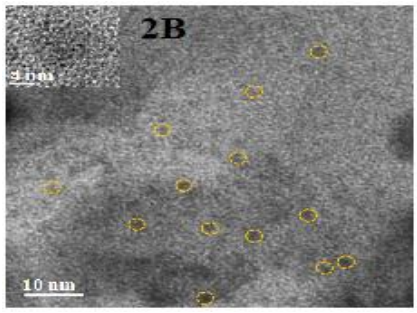

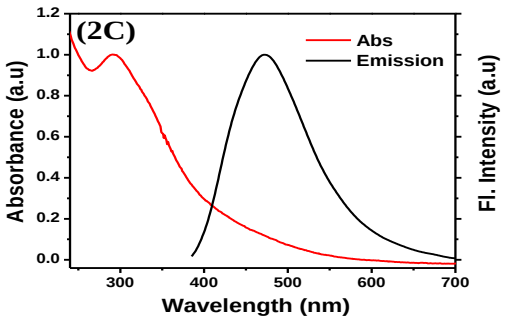

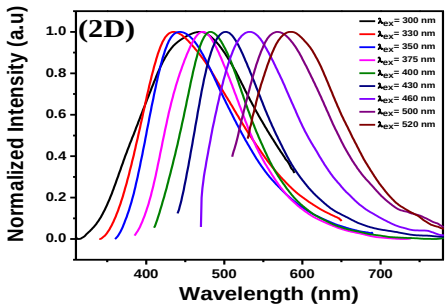

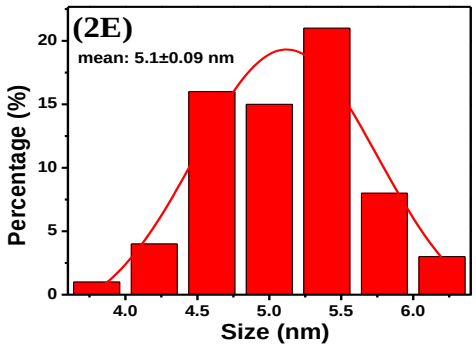

Fig. 2: (A) FTIR spectrum of PNDs. (B) HRTEM image of PNDs. (C) Absorption (red line) and normalized PL (black line) spectra of PNDs (λ_{ex}=375 nm). (D) Normalized PL spectra of PNDs at different excitation wavelength. (E) Size distribution histogram obtained from TEM measurements.

noticeable peak at 1388 cm^{-1} is assigned to the scissoring bending vibrations of C–H moieties. Estimated zeta potential of these synthesized CDs is ~1.52 mV at pH 7.4. Fig. 2B shows the high resolution transmission electron microscopy image (HRTEM) of the synthesized PNDs. From the HRTEM image of PNDs it is clear that they are well dispersed and spherical in shape. The inset of Fig. 2B shows the magnified image of a single PND. The corresponding particle size distribution histogram shown in Fig. 2E and it indicates that these particles have diameter ranging from 4 to 6 nm having mean diameter of 5.1±0.09 nm. The PNDs show an absorption maxima (λ_{abs}) at 291 nm which exactly matches with the earlier reported value. Excitation at 375 nm (λ_{ex}=375 nm) results in an intense photoluminescence band centered at 471 nm. Fig. 2C shows the combined absorption and emission spectra of the synthesized PNDs. Again the PNDs show excitation wavelength (λ_{ex}) dependence emission spectra and the emission maxima get red shifted (i.e. lower in energy) with rise in the excitation wavelength. Fig. 2D shows the

corresponding normalised emission spectra of PNDs at different excitation wavelength.

3.2 Steady state and time resolve measurements:

It is well known that the intrinsic fluorescence of BSA and HSA are mainly due to the presence of two Tryptophan residues at position 134 and 212 in sub-domain IB and IIA for BSA and one tryptophan residue at position 214 in sub-domain IIA for HSA. Upon excitation at 295 nm they show emission maxima at ~341 nm and ~337 nm respectively. Fig. 3A and Fig. 3B shows the fluorescence quenching of BSA and HSA respectively in presence of different concentration (in μM) of PNDs, obtained upon excitation at 295 nm. The emission maxima get red shifted (3 nm for BSA and 6 nm for HSA) due to gradual addition of PNDs.

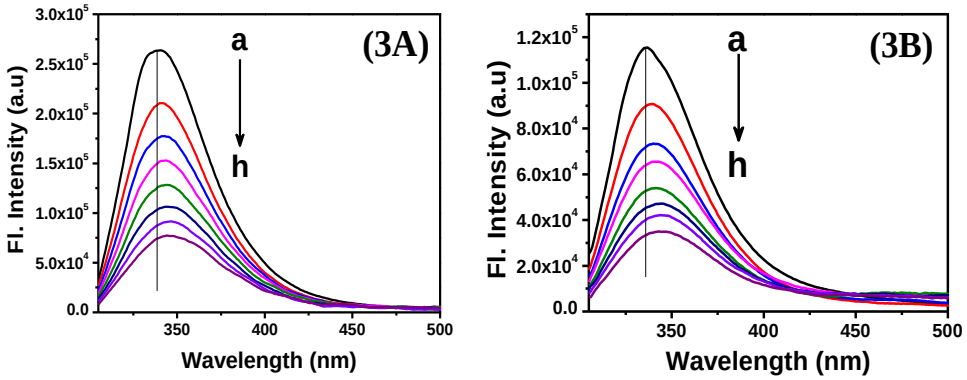

Fig. 3: Fluorescence spectra (λ_{ex}= 295 nm) of 2μM BSA and HSA (3A and 3B respectively) in 7.4 tris−HCl buffer at 298K in absence and presence of different concentration of PNDs. **a**-**h** BSA/HSA 2μM, PNDs 0, 0.64, 1.30, 1.94, 2.59, 3.23, 3.90, 4.53 μM.

For BSA the decrease of PL intensity is 68% while the same is 66% for HSA due to addition of 4.53μM PNDs. So, we can say that the quantum

yield of both BSA/HSA proteins retards significantly in presence of PNDs.

From the emission spectra of BSA/HSA it is clear that there must be some change in polarity near the Trp residues and that is why the emission maxima gets red shifted for both BSA and HSA. This may be due to unfolding (denaturation) of the serum albumin proteins in presence of PNDs. Since the PNDs has absorption at 295 nm along with the absorption of proteins so all the fluorescence spectres were OD corrected in presence of PNDs. *[45]* From the PL spectres of the proteins it is clear that there must be some association between the albumin proteins and PNDs and that leads to conformational changes of the proteins.

Now, any quenching phenomenon could be due to either static quenching or dynamic quenching or combination of both the quenching processes. Static and dynamic quenching can be identified with respect to temperature study as well as life time measurements. Since static quenching corresponds to ground state complex formation so with rise in temperature the extent of static quenching decreases because high temperature opposes the ground state complex formation. On the contrary in case of dynamic quenching excited state complex formation takes place. With rise in temperature the rates of diffusion of the components present in the system increases and this leads to effective increase in the collision and thereby the extent of dynamic quenching increases significantly. Now it is easier to explain any quenching process with respect to mechanistic facts and quenching parameters by the well known Stern-Volmer (SV) equation, as follows:

$$\frac{F_0}{F} = 1 + K_{sv}[Q] = 1 + k_q \tau_0 [Q]$$

where F_0 and F are the fluorescence intensities in the absence and presence of a quencher (here PNDs). K_{SV} is the Stern–Volmer (SV) constant and [Q] is the molar concentration of quencher. k_q is the bimolecular quenching rate constant and τ_0 is the fluorescence lifetime of

the fluorophore (here BSA/HSA) in the absence of a quencher. The Stern-Volmer constant and quenching rate constant can be evaluated from a plot of F_0/F against [Q]. Fig. 4A and Fig. 4B shows the steady state Stern-Volmer plot of BSA/HSA with respect to different concentration of PNDs at three different temperatures 298K, 308K and 318K. Calculated SV constants are listed in table 2. At 298K the bimolecular quenching constant k_q has been calculated for BSA/HSA from the SV constant (Table 2) and τ_0 of BSA and HSA as 0.85×10^{14} $M^{-1}S^{-1}$ and 0.75×10^{14} $M^{-1}S^{-1}$

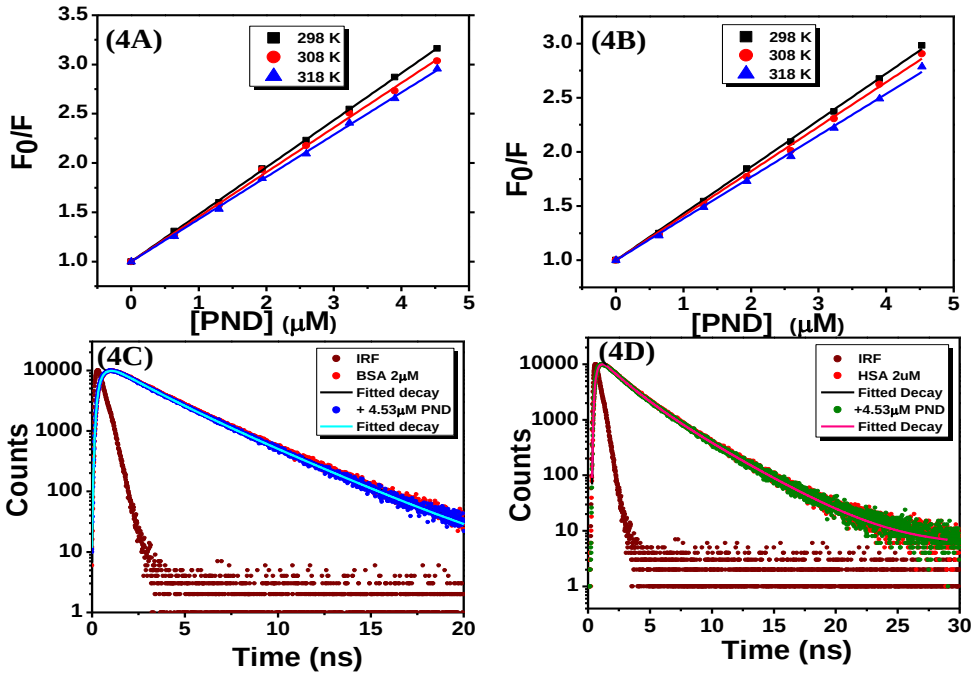

Fig. 4: (4A/4B) Steady-state Stern-Volmer plot at three different temperatures (298K, 308K and 318K) for BSA and HSA respectively. (4C/4D) Life time decay curves (λ_{ex}=278 nm) of 2μM BSA and HSA respectively in 7.4 tris-HCl buffer at 298K in absence and presence of 4.53μM PNDs.

(for BSA K_{SV} = 4.78×10^5 M^{-1} and τ_0 = 5.62 ns and for HSA K_{SV} = 4.30×10^5 M^{-1} and τ_0 = 5.72 ns) which is four orders of magnitude higher than that for a purely dynamic quenching mechanism. *[46,47]* Hence, in

the present system the observed fluorescence quenching of BSA/HSA by PNDs might be due to static ground state complex formation and not due to collisional encounter. Moreover some example of static quenching mechanism has been proposed earlier for other protein−NP association processes. *[48-51]*

Protein	T(K)	K_{sv} ($10^5 M^{-1}$)	K_b ($10^5 M^{-1}$)	n	R^2	ΔG (kJ mol^{-1})	ΔH ($kJmol^{-1}$)	ΔS ($JK^{-1}mol^{-1}$)
BSA	298	4.78	5.01	1.07 ± 0.01	0.998	-32.43	-49.60 ±1.50	-57.62
	308	4.34	2.63	1.00 ± 0.01	0.998	-31.85		
	318	3.95	1.32	0.97 ± 0.01	0.998	-31.28		
HSA	298	4.30	8.13	1.07 ± 0.01	0.998	-33.75	-54.39 ±2.06	-69.25
	308	3.88	4.16	1.05 ± 0.01	0.998	-33.06		
	318	3.48	2.81	0.99 ± 0.01	0.998	-32.36		

Table 2: Stern–Volmer quenching constant (K_{SV}), binding constants (K_b), the number of binding sites (n) and thermodynamic parameters for the BSA/HSA–PNDs complexes.

Fluorescence lifetime serves as a sensitive parameter for sensing the local environment around a fluorophore, and it is sensitive to the interactions in the photo-excited state. *[52]* It also allows one to understand the interaction

between probe and proteins. *[53]* Despite the fact that the structure of HSA is rather complicated, it has been widely studied by making use of the single Trp-214 residue enabling the serum protein to act as an intrinsic fluorophore. In aqueous solution at neutral pH, Trp- 214 exhibits multiple exponential decays, attributed to the existence of rotational conformational isomers, called rotamers. *[54]* Time-resolved lifetime measurements have been performed to get further proof for the dynamics of the BSA/HSA-PNDs complexes along with the change of lifetime of the proteins in the excited state in presence of PNDs. Fig. 4C and Fig. 4D displays the typical lifetime decays of BSA/HSA in the absence and presence of maximum concentration of PNDs. In the absence of PNDs, BSA/HSA shows a biexponential decay curve with an average lifetime of 5.62 ns (having lifetime components of 4.36 and 7.3) and 5.72 ns (having lifetime components of 3.51 and 6.58) respectively and these values are quite similar with the earlier reported value.*[55]* The decay curve of BSA/HSA remains unaltered in the presence of maximum concentration of PNDs. The fluorescence decay of BSA/HSA remains biexponential in the presence of 4.53μM PNDs with an average lifetime of 5.56 ns (having lifetime components of 3.65 and 7.44) and 5.69 ns (having lifetime components of 3.37 and 6.64) respectively. The lifetime decay parameters are shown in Table 3. Although the average lifetime of BSA/HSA does not change significantly in the presence of PNDs, it is important to note the small change observed in average lifetime of BSA/HSA from 5.62 ns to 5.56 ns and 5.72 ns to 5.69 ns respectively. This low decrease in lifetime in the presence of the highest concentration of PNDs used in the present study could be due to the local conformational alterations of BSA/HSA upon adsorption on PNDs surface.

Sample	a_1	τ_1(ns)	a_2	τ_2(ns)	$\langle\tau\rangle$(ns)	χ^2
BSA 2µM	0.57	4.36	0.43	7.3	5.62	1.07
BSA2µM+4.53 µM PND	0.58	3.65	0.42	7.44	5.56	1.08
HSA 2µM	0.28	3.51	0.72	6.58	5.72	1.09
HSA2µM+4.53 µM PND	0.29	3.37	0.71	6.64	5.69	1.06

	a_1	τ_1	a_2	τ_2	a_3	τ_3	$<\tau>$	χ^2
PNDs	0.29	2.57	0.16	9.86	0.55	3.79	2.56	1.13

Table 3: Fluorescence lifetime components of BSA and HSA (λ_{ex}=278nm) at 298K in absence and presence of maximum concentration of PNDs.

Now we know that BSA has two Tryptophan moieties (Trp-134 and Trp-212) and HSA has only one (Trp-214). The two Trp residues of BSA are present in two different domains with some obvious different microenvironment. Trp-134 is located at the surface of the protein in sub-domain IB while Trp-212 is located in the hydrophobic cavity of sub-domain IIA. The Trp-214 for HSA present in the same hydrophobic cavity of sub-domain IIA microenvironment. Hydrophobic interactions will lead to binding of NPs at the hydrophobic binding pocket at sub-domain IIA near Trp-212/Trp-214 while electrostatic; hydrogen bonding interactions will lead to binding near the Trp-134 residue. *[59]* Therefore it is important which Trp moiety of BSA gets quenched during the association process with PNDs and what actually happens of the Trp of HSA with PNDs. To clarify this basic question we calculated various thermodynamic parameters (ΔG, ΔH and ΔS), which have been discussed in the following section.

3.3 Effect of temperature and thermodynamics of binding:

The association of BSA and HSA with PNDs in the ground state were established by studying the PNDs induced quenching of BSA/HSA. In a system involving static quenching process, when small molecules (NPs) bind independently to a set of equivalent sites on a macromolecule, we can investigate the probable interaction from the binding constant (K_b) and the number of binding sites (n) by monitoring temperature of the system. Here we have calculate K_b and n (see table 2) at three different temperature 298K, 308K and 318K according to the Scatchard equation*[56]* as follows:

$$\log\left(\frac{F_0 - F}{F}\right) = \log K_b + n\log[Q]$$

where K_b is the binding constant of the BSA/HSA-PND complex and n is the number of binding sites. The plot of $\log\left(\frac{F_0 - F}{F}\right)$ vs. log [Q] gives a straight line having slope n and intercept $\log K_b$. From the intercept we can calculate binding constant (K_b) and from the slope we can get the number of binding sites (n). Fig. 5A and Fig. 5B shows the plot of $\log\left(\frac{F_0 - F}{F}\right)$ against log [PNDs] at three different temperatures which shows a linear relationship with a slope equal to n. The estimated binding constant for the BSA/HSA–PNDs systems are $5.01\pm0.10\times10^5$ M^{-1} and $8.13\pm0.10\times10^5$ M^{-1} respectively at 298K (see Table 2). The number of binding sites for PNDs is approximately equal to one for both BSA and HSA. The binding constants for the BSA/HSA–PNDs systems decrease with increase in temperature, indicating the static nature of the complexes. Furthermore, the observed values complement the findings of 1:1 binding stoichiometry for both the complexes.

The interaction forces between PNDs and bio-molecules may include electrostatic interactions, multiple hydrogen bonds,

Van-der-Waals interactions, hydrophobic and steric contacts within the antibody-binding site, and so on. If the enthalpy change (ΔH) doesn't vary significantly in the temperature range studied, both the enthalpy change (ΔH) and entropy change (ΔS) can be evaluated from the Van't Hoff equation:

$$\ln K_b = \frac{\Delta S}{R} - \frac{\Delta H}{RT}$$

where K_b is analogous to the associative binding constants at the corresponding temperatures and R is the universal gas constant. To elucidate the interaction between PNDs and BSA/HSA, the thermodynamic parameters were calculated from the Van't Hoff equation (Fig. 5C and 5D). ΔS and ΔH are calculated from the intercept and slope of the $\ln K_b$ vs 1/T plot at different temperature. Then the Gibbs free energy change (ΔG) can be estimated from the following Gibbs-Helmholtz relationship:

$$\Delta G = \Delta H - T\Delta S$$

The calculated thermodynamic parameters for the present system are listed in Table 2. The negative values of free energy (ΔG), supports that the association phenomenon is spontaneous. It was reported earlier that positive entropy (ΔS) and positive enthalpy (ΔH) values generally represents hydrophobic interactions. *[57, 58]* On the other hand association processes triggered by electrostatic interactions proceed with a positive entropy change with a small positive or negative enthalpy change. *[57]* But, in our present study thermodynamic parameters are not correlated with either of these two approaches.

There are some previous reports associated with negative enthalpy change with a negative entropy in many association processes and has been assigned to involvement of specific hydrogen bonding interactions. *[57, 59]* It should be remember that the surface charge (Zeta potential) and size of the NPs are the key factors for the thermodynamic parameters.

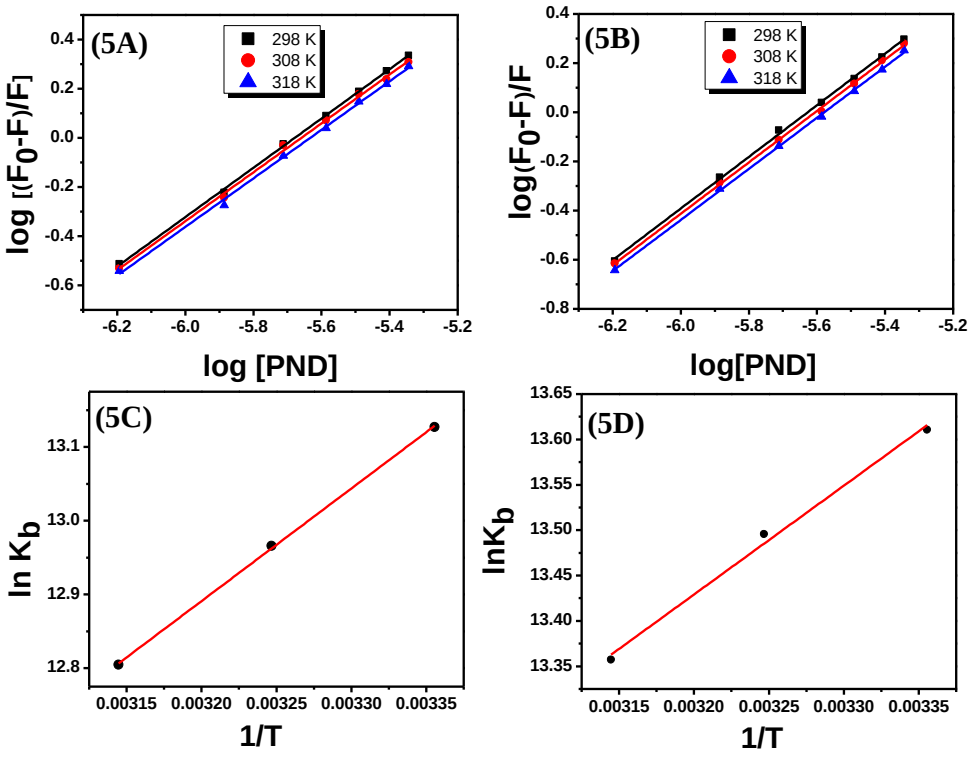

Fig. 5: (5A/5B) Scatchard plots for BSA/HSA−PNDs system at three different temperatures. (5C/5D) Van't−Hoff plots for the same.

Both BSA and HSA has iso-electric point 4.7 in water so at pH 7.4 they act as a negatively charged proteins since the –COOH groups exist as –COO^- at this pH. Domain I is more negatively charged than domain II, while domain III is completely neutral for both the proteins. *[60]* Thus from the above thermodynamic parameters we can conclude that association of BSA and HSA on the surface of PNDs arises due to specific H-bonding interactions between amine (–NH_2) and hydroxyl (–OH) groups of PNDs and carboxylate (–COO^-) groups of aspartate and glutamate amino acids of BSA/HSA present in domain I and domain II (scheme 2). The unfavourable negative entropy change during the adsorption process may be due to the conformational restriction of BSA and HSA with PNDs.

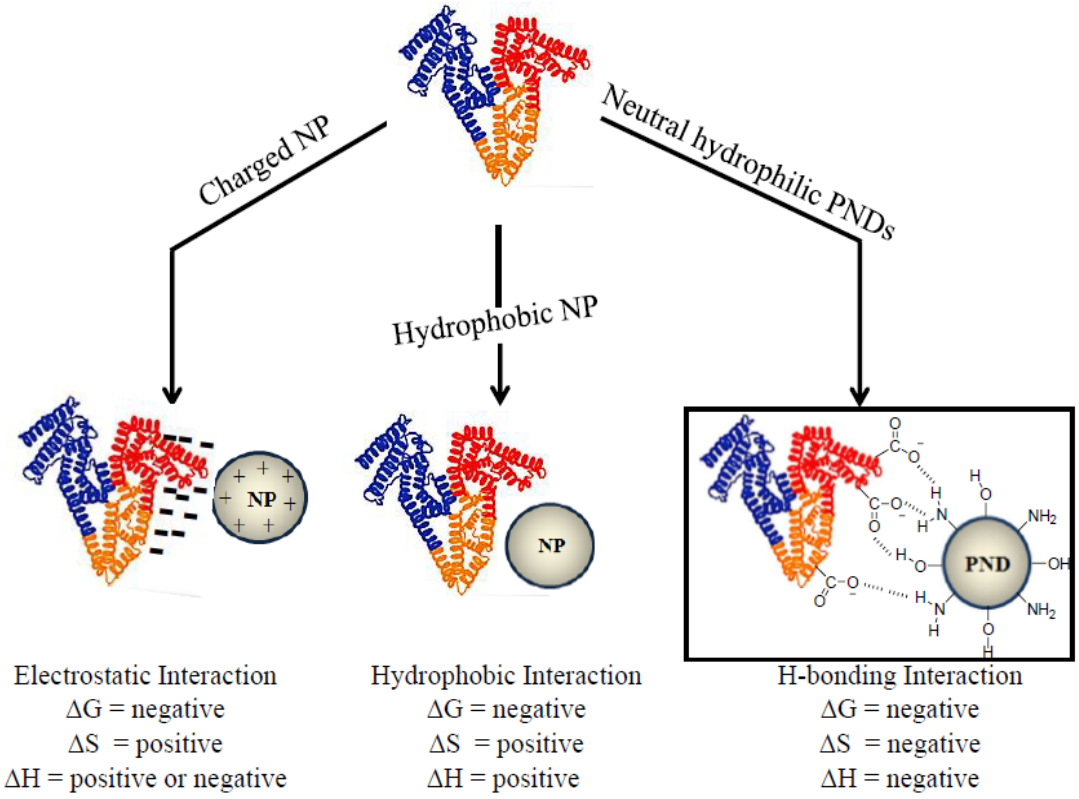

Scheme 2: Schematic representation of the association of serum albumins with different kind NPs and the PNDs surface driven by electrostatic, hydrophobic or H-bonding interactions. The thermodynamic parameters vary with different types of interactions. The present proposed model is highlighted in the scheme.

3.4 Study for electrostatic interaction; Salt-effect:

To see whether the association of BSA/HSA with PNDs are electrostatic or not we have done PL study of BSA and HSA in presence of a salt solution. Fig. 6A, 6B, 6C and 6D depicts the emission spectra of BSA and HSA respectively upon excitation at 295 nm in presence and absence of 150μM NaCl solution. Upon addition of maximum concentration of PNDs

the emission intensity of both BSA and HSA decreases in presence and absence of NaCl solution. Now, F_0/F (where F_0 and F are the emission

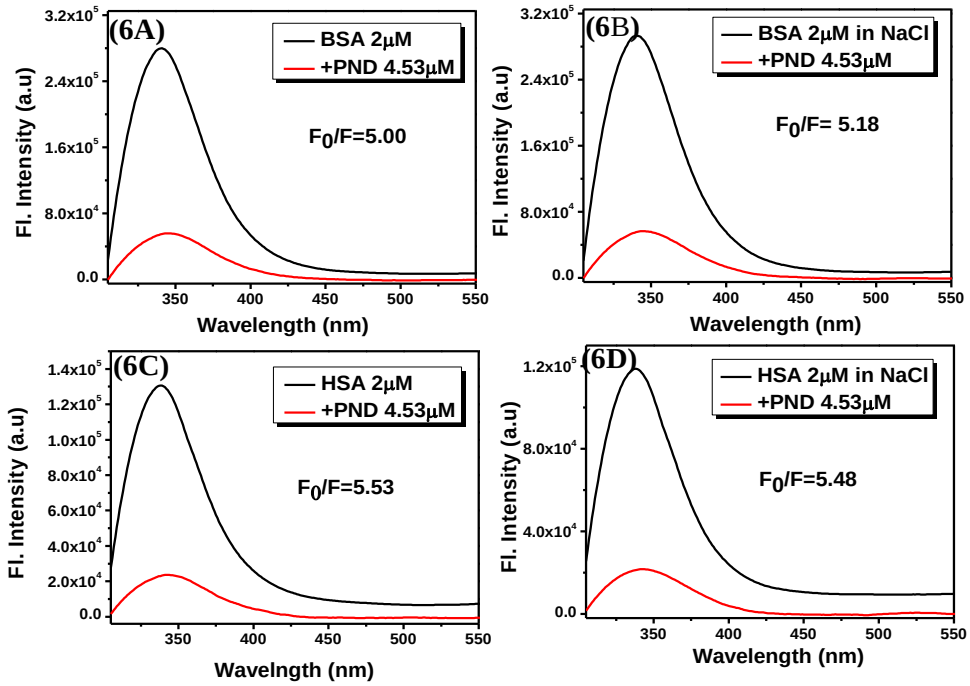

Fig. 6: Fluorescence quenching of 2μM BSA/HSA in absence and presence of NaCl solution (6A and 6B for BSA and 6C and 6D for HSA) upon addition of maximum concentration of PNDs. F_0/F ratios are shown within the plots.

intensity of BSA/HSA in absence and presence of PNDs) calculation of all the fluorescence studies (Fig. 6A to 6D) shows that the extent of PL quenching for BSA/HSA is almost same whether they are present in NaCl solution or simply in buffer medium. Since the extent of quenching is more or less same for both the cases so we can conclude that there is no electrostatic interaction between the albumin proteins and PNDs.

3.5 Site marker-competitive binding experiments:

BSA/HSA has a limited number of binding sites for many endogenous and exogenous ligands that can typically bound reversibly with binding constants of 10^4 to 10^8 M^{-1}. *[61]* As indicated in the introduction, there are three regions in the BSA/HSA protein for the binding of small molecules, i.e. domains I, II and III, each containing two sub-domains A and B. *[34]* The principal binding sites on BSA/HSA are located in hydrophobic cavities in sub-domains IIA and IIIA (also referred to as site I and site II), which exhibit similar chemical properties. The binding locations are commonly studied with ligand markers, such as the two used in this study− warfarin (Waf) and ibuprofen (Ibu), as fluorescent probes for site I and site II respectively. To identify the binding sites of BSA/HSA during the associated during the complex formation with PNDs site marker competitive experiments are carried out using the two drags warfarin and ibuprofen, and they are specifically bind to a particular site on BSA/HSA.

During the site selective binding study, PNDs of different concentration was gradually added to a solution of BSA/HSA and site markers held in equimolar concentrations (2μM). Because of addition of warfarin into BSA, the emission maxima of BSA had shown (Fig. 7A) an obvious red shift (from 341 nm to 348 nm), and the fluorescence intensity was significantly lower than the intrinsic fluorescence of BSA. Now, with the addition of PNDs, the fluorescence of BSA gradually decreases accompanied with ~12 nm red shifting of the emission maxima. On the other hand in case of HSA addition of warfarin (Fig. 7C) increases the fluorescence intensity significantly with a large red shift (from 335 nm to 368 nm) of the emission maxima. After addition of PNDs the fluorescence intensities of HSA gradually decreases with ~11 nm red shift of the emission maxima. This suggests an increased polarity around the periphery of Trp-212 and Trp-214 (domain IIA) for BSA and HSA respectively and indicating that the association of BSA/HSA on the PNDs surface were obviously affected by adding warfarin. On the other hand

Fig. 7B and 7D shows the comparison of the fluorescence spectra of BSA/HSA-PNDs system in presence of ibuprofen. In contrast, in the presence of ibuprofen, the fluorescence property of the BSA/HSA remains almost the same as in the absence of it and after continuous addition of PNDs progressively decreases the fluorescence intensity of both the

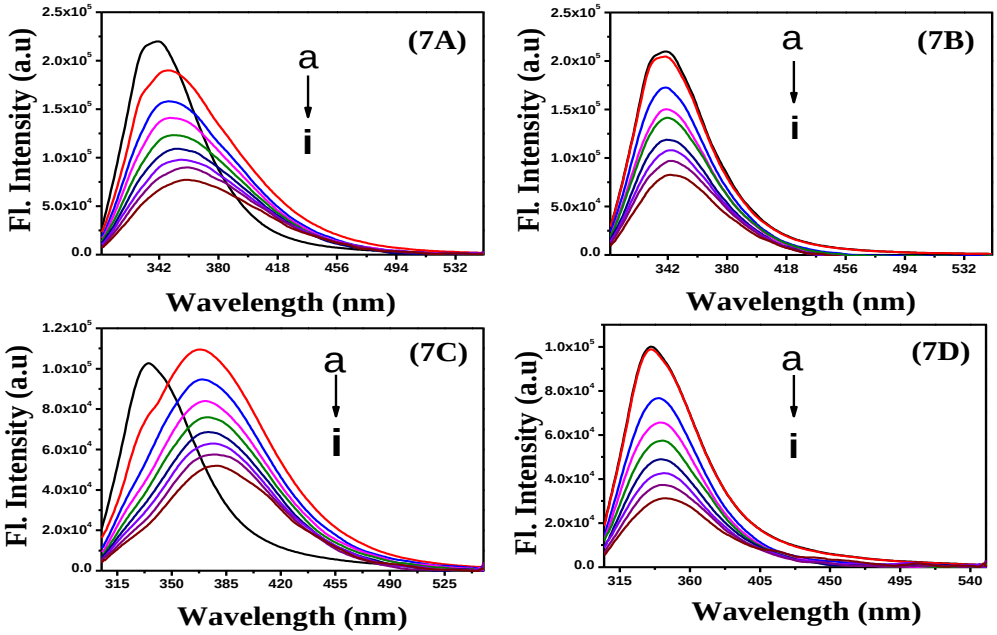

Fig. 7: Effect of PNDs on the intrinsic fluorescence of BSA (7A and 7B) and HSA (7C and 7D) in presence of site markers warfarin and ibuprofen. **a-i** BSA/HSA 2µM, Waf/Ibu 2µM, PNDs 0, 0, 0.64, 1.30, 1.94, 2.59, 3.23, 3.90, 4.53 µM.

serum albumins, which indicated that ibuprofen did not prevent the binding of PNDs in its usual binding position.

To compare the influence of warfarin and ibuprofen on the adsorption of BSA and HSA on PNDs surface, the binding constants in the presence and absence of the site markers were further analyzed with the help of Scatchard equation (See Table 4). The results show that the binding constant was abruptly changes in presence of warfarin, while a

Proteins	Sample	Binding constant(K_b,M^{-1})
BSA	Blank	5.01×10^5
	BSA+Waf+PND	2.13×10^5
	BSA+Ibu+PND	4.07×10^5
HSA	Blank	8.13×10^5
	HSA+Waf+PND	1.99×10^5
	HSA+Ibu+PND	5.12×10^5

Table 4: Binding constants of the competitive experiments in presence of site markers at 298K.

small change in binding constant is observed in presence of ibuprofen (somewhat lower than with isolated BSA/HSA). Thus, the results indicated that the association of BSA and HSA on the surface of PNDs selectively takes place through site I (sub-domain IIA) of the proteins, and the decrease in probe fluorescence may result from competitive displacement of the probe.

3.6 Secondary structure of BSA/HSA in presence of PNDs:

Circular Dichroism (CD) spectroscopy is widely used to monitor the structural, conformational change as well as the stability of large biological systems. *[62-64]* It deals with the secondary structure of proteins although it does not provide the details regarding the precise structure. Fluorescence techniques are rather more sensitive for small changes at molecular level. *[65]* Here, in order to know the conformational changes of BSA/HSA due to surface adsorption on PNDs as well as in presence of warfarin we have done the far-UV CD spectra for both the proteins. The CD spectral analysis of BSA/HSA exhibit (Fig. 8A and Fig. 8B) a typical shape of an α-helix rich secondary structure (two

minima at approximately 208 and 222 nm at pH 7.4). *[66-68]* The CD spectrum of free BSA/HSA shows a strong negative ellipticity at 208 and

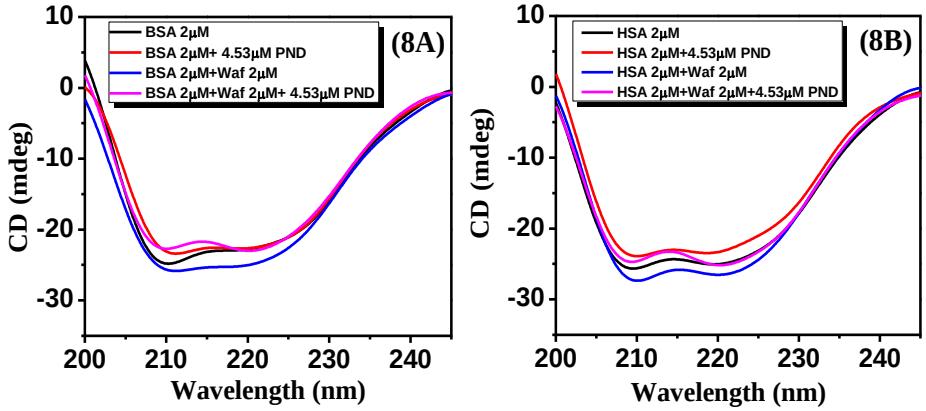

Fig. 8: (8A/8B) The CD spectra changes for BSA and HSA in absence and presence of PNDs and warfarin respectively.

222 nm. From the CD spectra of BSA/HSA it is clear that in presence of PNDs the secondary structure of both the serum albumins change, as it is found that due to addition of PNDs the CD signal of BSA/HSA increases with no significant shift of the two minima points. The α-helical content of BSA and HSA was evaluated by the following equation: *[69]*

$$\alpha - Helix(\%) = \frac{-(MRE_{222} - 2340)}{30300} \times 100$$

where MRE is the mean residual ellipticity and MRE_{222} is the observed MRE value at 222 nm which is again calculate by the following relation:

$$MRE_{222} = \frac{ObservedCD(m\deg)}{[C_p nl \times 10]}$$

C_p is the molar concentration of the protein, n is the number of amino acid residues (583 amino acid residues for BSA and 585 amino acid residues for HSA), l is the path length of the cell used (0.1 cm). The secondary structural analysis (see Table 5) however shows that the α-helix content

for both BSA and HSA loses from 64.65% to 55.58% and 66.43% to 60.11% respectively in presence of maximum concentration of PNDs. These spectral changes demonstrate significant alteration (9.07% loss for BSA and 6.32% loss for HSA helicity) in the secondary structure of BSA and HSA. There are several reports which suggest that strong electrostatic interactions between protein and NPs result in considerable structural alteration of the native conformation due to columbic attractions. *[70, 71]* The structure and stability of BSA/HSA on various NP surfaces have also been explored in great detail.

Protein	Sample	α-helix (%)
BSA	BSA 2µM	64.65
	BSA 2µM+4.53µM PND	55.58
	BSA 2µM+Waf 2µM	67.05
	BSA 2µM+Waf 2µM+4.53µM PND	59.03
HSA	HSA 2µM	66.43
	HSA 2µM+4.53µM PND	60.11
	HSA 2µM+Waf 2µM	69.80
	HSA 2µM+Waf 2µM+4.53µM PND	63.58

Table 5: Secondary structure analysis of BSA and HSA in presence and absence of maximum concentration of PNDs and site markers.

However, in the present study the observed changes in the secondary structure of BSA/HSA on the PNDs surface is believed due to partial unfolding of native protein. From our present study we propose a model where specific H-bonding interaction takes place between the surface exposed $–COO^-$ groups of aspartate (Asp) and glutamate (Glu) residues of BSA/HSA with amine ($–NH_2$) and hydroxy (-OH) moieties of PNDs drive the association process. It is also important to mention that the tertiary structure of both the proteins remain unchanged during the association process.

Chapter 4:

4.1 CONCLUSION:

In this work, we have demonstrated the specific interaction of PNDs with BSA and HSA spectroscopically. The lifetime and temperature-dependent experiments indicate that the fluorescence quenching observed for BSA and HSA in presence of PNDs is due to the static quenching mechanism i.e. a ground state complex formation takes place between them and this complex formation is spontaneous. Salt effect experiments suggest that electrostatic interaction do not play any major role during the ground state complex formation. The calculated thermodynamic parameters (negative ΔH and negative ΔS values) demonstrate that a specific hydrogen bonding interaction is present between amine ($–NH_2$)/hydroxyl (-OH) groups of PNDs with carboxylate ($–COO^-$) groups of aspartate (Asp) and glutamate (Glu) residues of BSA/HSA. Site marker competitive experiment indicates that association of BSA/HSA with PNDs selectively takes place through site I (domain II). Circular dichroism (CD) spectra revealed considerable alteration in the secondary structure of BSA and HSA on the PNDs surface because of partial unfolding of the proteins although the tertiary structure remains unchanged.

References:

1. R.H. Liu, H.T. Li, W.Q. Kong, J. Liu, Y. Liu, C.Y. Tong, X. Zhang and Z. H. Kang, *Mater. Res. Bull*., 2013, **48,** 2529–2534.
2. C.J. Liu, P. Zhang, F. Tian, W.C. Li, F. Li and W.G. Liu, *J. Mater. Chem.*, 2011, **21**, 13163–13167.
3. F. Wang, Y.H. Chen, C.Y. Liu and D.G. Ma, *Chem. Commun.*, 2011, **47**, 3502–3506.
4. Y. Li, B.P. Zhang, J.X. Zhao, Z.H. Ge, X. K. Zhao and L. Zou, *Appl. Surf. Sci.*, 2013, **279**, 367–373.
5. J. Shen, Y. Zhu, X. Yang and C. Li, *Chem. Commun.*, 2012, **48**, 3686–3699.
6. X. Y. Xu, R. Ray, Y.L. Gu, H. J. Ploehn, L. Gearheart, K. Raker and W.A. Scrivens, *J. Am. Chem. Soc.*, 2004, **126**, 12736–12737.
7. X. H. Gao, Y. Y. Cui, R. M. Levenson, L. W. K. Chung and S.M. Nie, *Nat. Biotechnol.*, 2004, **22**, 969–976.
8. S. Yao, Y. F. Hu and G. K. Li, *Carbon*, 2014, **66**, 77–83.
9. Y. Liu, C. Y. Liu and Z. Y. Zhang, *Appl. Surf. Sci.*, 2012, **263**, 481–485.
10. S. N. Baker and G. A. Baker, *Angew. Chem., Int. Ed.*, 2010, **49**, 6726–6744.
11. Y. Wang, S. Kalytchuk, Y. Zhang, H. Shi, S. V. Kershaw and A. L. Rogach, *J. Phys. Chem. Lett.*, 2014, **5**, 1412–1420.
12. S. Zhang, J. Li, M. Zeng, J. Xu, X. Wang and W. Hu, *Nanoscale*, 2014, **6**, 4157.
13. S. Liu, J. Tian, L. Wang, Y. Zhang, X. Qin, Y. Luo, A. M. Asiri, A. O. Al-Youbi, X. Sun, *Adv. Mater.*, 2012, **24**, 2037–2041.
14. J. Zhou, C. Wang, Z. S. Qian, C. C. Chen, J. J. Ma, G. H. Du, J. R. Chen and H. Feng, *J. Mater. Chem.*, 2012, **22**, 11912.
15. B. Uchoa and A. H. C. Neto, *Phys. Rev. Lett.*, 2007, **98**, 146801.

16. A. L. M. Reddy, A. Srivastava, S. R. Gowda, H. Gullapalli, M. Dubey and P. M. Ajavan, *ACS Nano*, 2010, **4**, 6337.
17. X. H. Wang, K. G. Qu, B. L. Xu, J. S. Ren and X. G. Qu, *Nano Research*, 2011, **4**, 908–920.
18. J. H. Shen, Y. H. Zhu, X. L. Yang and C. Z. Li, *Chem. Commun.*, 2012, **48**, 3686–3699.
19. S. Liu, J. Q. Tian, L. Wang, Y. L. Luo, J. F. Zhai and X. P. Sun, *J. Mater. Chem.*, 2011, **21**, 11726.
20. P. C. Hsu and H. T. Chang, *Chem. Commun.*, 2012, **48**, 3984.
21. Z. C. Yang, X. Li and J. Wang, *Carbon*, 2011, **49**, 5207.
22. J. Jiang, Y. He, S. Y. Li and H. Cui, *Chem. Commun.*, 2012, **48**, 9634.
23. S. Kumar, A. K. Rai, V. B. Singh and S. B. Rai, *Spectrochim. Acta*, Part A, 2005, **61**, 2741.
24. D. T. Sawyer and J. M. McKinnie, *J. Am. Chem. Soc.*, 1960, **82**, 4191.
25. S. Schroetter-Dirks and D. Bougeard, *J. Mol. Struct.*, 2003, **661**, 109.
26. Y. Kamio, Y. Itoh, Y. Terawaki and T. Kusano, *J. Bacteriol.*, 1981, **145**, 122.
27. Y. H. Yang, J. H. Cui, M. T. Zheng, C. F. Hu, S. Z. Tan, Y. Xiao, Q. Yang and Y. L. Liu, *Chem. Commun.*, 2012, **48**, 380.
28. D. Y. Pan, J. C. Zhang, Z. Li and M. H. Wu, *Adv. Mater.*, 2010, **22**, 734.
29. S. Liu, J. Q. Tian, L. Wang, Y. W. Zhang, X. Y. Qin, Y. L. Luo, A. M. Asiri, A. Y. Abdulrahman and X. P. Sun, *Adv. Mater.*, 2012, **24**, 2037.
30. T. J. Peters, Genetics and Medicinal Applications, Academic Press, San Diego, CA, 1996.
31. Hu. Y. J, Liu. Y and Xiao X. H, *Biomacromolecule, 2009,* **10,** 517.
32. Min. H. X and Carter. D. C, *Nature,* 1992, **358** 209.

33. T. Peters Advances in Protein Chemistry, Academic Press, New York, 1985.
34. M. K. Helms, C. E. Peterson, N. V. Bhagavan and D. M. Jameson, *FEBS Lett.*, 1997, **408**, 67–70.
35. M. E. Kemary, M. Gil and A. Douhal, *J. Med. Chem.*, 2007, **50**, 2896–2902.
36. Jiménez, M. C., Miranda, M. A, and Vayá, I., *J. Am. Chem. Soc*., 2005, **127**, 10134-10135.
37. Lhiaubet-Vallet V., Sarabia Z., Boscá. F and Miranda M. A., *J. Am. Chem. Soc***.,** 2004, **126**, 9538-9539.
38. Sudlow. G., Birkett. D. J and Wade D. N., *Mol. Pharmacol.* 1975, **11**, 824–832.
39. Sudlow, G., Birkett D. J. and Wade D. N., *Mol. Pharmacol.* 1976, **12**, 1052–1061.
40. Wanwimolruk, S., Birkett D. J. and Brooks P. M., *Mol. Pharmacol.* 1983, **24**, 458–463.
41. T. Lai, E. Zheng, L. Chen, X. Wang, L. Kong, C. You, Y. Ruan and X. Weng, *Nanoscale*, 2013, **5**, 8015–8021.
42. S. Zhu, Q. Meng, L. Wang, J. Zhang, Y. Song, H. Jin, K. Zhang, H. Sun, H. Wang and B. Yang, *Angew. Chem. Int. Ed*., 2013, **52**, 3953–3957.
43**.** N. J. Turro, V. Ramamurthy and J. C. Scaiano, Modern molecular photochemistry of organic molecules, 2015.
44. B. Birdsall, R. W. King, M. R. Wheeler, C. A. Lewis Jr, S. R. Goode, B. Dunlap and G. C. K. Roberts, *Anal. Biochem.*, 1983, **132**, 353–361.
45. Birdsall. B., King. R. W., Wheeler. M. R., Lewis. C. A., Jr. Goode, S. R. Dunlap, B. and Roberts G. C. K, *Anal. Biochem.*, 1983, **132**, 353−361.
46. W. R. Ware, *J. Phys. Chem.*, 1962, **66**, 455–458.
47. M. Tachiya, *Chem. Phys. Lett.*, 1986, **127**, 55–59.

48. S. Chakraborti, S. Sarwar and P. Chakrabarti, *J. Phys. Chem. B*, 2013, **117**, 13397–13408.
49. S. Chakraborti, P. Joshi, D. Chakravarty, V. Shanker, Z. A. Ansari, S. P. Singh and P. Chakrabarti, *Langmuir*, 2012, **28**, 11142–11152.
50. S. Chakraborti, T. Chatterjee, P. Joshi, A. Poddar, B. Bhattacharyya, S. P. Singh, V. Gupta and P. Chakrabarti, *Langmuir*, 2010, **26**, 3506–3513.
51. M. Losin, V. Canpean and S. Astilean, *J. Photochem. Photobiol. A*, 2011, **217**, 395–401.
52. Das. P, Mallick. A, Haldar. B, Chakrabarty. A and Chattopadhyay. N, *J. Chem. Phys.*, 2006 **125,** 044516.
53. Patel. S and Datta. A, *J. Phys. Chem.* B, 2007, **111,** 10557.
54. Lakowicz. J. R, *Principles of fluorescence spectroscopy* (ed.), 2006, (New York: Springer).
55. U. Anand and S. Mukherjee, *Phys. Chem. Chem. Phys.*, 2013, **15**, 9375–9383.
56. E. Lissi, C. Calderon and A. Campos, *Photochem. Photobiol.*, 2013, **89**, 1413–1416.
57. P. D. Ross and S. Subramanian, *Biochemistry*, 1981, **20,** 3096–3102.
58. Timaseff. S. N., Thermodynamics of protein interactions. In *Proteins of biological fluids*; Peeters, H., Ed.; Pergamon Press: Oxford, 1972.
59. S. Chatterjee and T. K. Mukherjee, *Phys.Chem.Chem.Phys.*, 2014, **16**, 8400.
60. K. Hansen, *U. Pharmacol. ReV.*, 1981, **33**, 17–53.
61. W. Y. He, Y. Li, J. Q. Liu, Z. D. Hu and X. G. Chen, *Biopolymers*, 2005, **79**, 48–57.
62. Moriyama. Y and Takeda. K, *Langmuir*, 1999, **15,** 2003.
63. Moriyama. Y and Takeda. K, *Langmuir*, 2005, **21,** 5524.
64. Parker. W and Song. P. S, *Biophys. J.*, 1992, **61,** 1435.

65. Anand. U, Jash. C and Mukherjee S, *J. Phys. Chem. B*, 2010, **114,** 15839.

66. Charbonneau. D., Beauregard. M., Tajmir-Riahi. H. A., *J. Phys. Chem. B*, 2009, **113,** 1777–1784.

67. Lu. G., Ai. S., Li. J., *Langmuir*, 2005, **21**, 1679–1682.

68. Sen. P., Fatima. S., Ahmad. B. and Khan. R. H., *Spectrochim. Acta, Part A*, 2009, **74,** 94–99.

69. S. M. Kelly, T. J. Jess and N. C. Price, *Biochim. Biophys. Acta*, 2005, **1751(2)**, 119–139.

70. W. Shang, J. H. Nuffer, J. S. Dordick and R. W. Siegel, *Nano Lett*., 2007, **7**, 1991–1995.

71. A. A. Vertegel, R. W. Siegel and J. S. Dordick, *Langmuir*, 2004, **20**, 6800–6807.